NAVAL POSTGRADUATE SCHOOL

MONTEREY, CALIFORNIA

THESIS

AN EXPERIMENTAL STUDY OF STEADY STATE HIGH HEAT FLUX REMOVAL USING SPRAY COOLING

by

James B. Fillius

December 2004

Thesis Advisor: Ashok Gopinath

Approved for public release; distribution is unlimited

THIS PAGE INTENTIONALLY LEFT BLANK

REPORT DOCUMENTATION PAGE			Form Approved OMB No. 0704-0188
Public reporting burden for this collection of information is estimated to average 1 hour per response, including the time for reviewing instruction, searching existing data sources, gathering and maintaining the data needed, and completing and reviewing the collection of information. Send comments regarding this burden estimate or any other aspect of this collection of information, including suggestions for reducing this burden, to Washington headquarters Services, Directorate for Information Operations and Reports, 1215 Jefferson Davis Highway, Suite 1204, Arlington, VA 22202-4302, and to the Office of Management and Budget, Paperwork Reduction Project (0704-0188) Washington DC 20503.			
1. AGENCY USE ONLY ***(Leave blank)***	**2. REPORT DATE** December 2004	**3. REPORT TYPE AND DATES COVERED** Master's Thesis	
4. TITLE AND SUBTITLE: An Experimental Study of Steady State High Heat Flux Removal Using Spray Cooling			**5. FUNDING NUMBERS**
6. AUTHOR(S) James B. Fillius			
7. PERFORMING ORGANIZATION NAME(S) AND ADDRESS(ES) Naval Postgraduate School Monterey, CA 93943-5000			**8. PERFORMING ORGANIZATION REPORT NUMBER**
9. SPONSORING /MONITORING AGENCY NAME(S) AND ADDRESS(ES) N/A			**10. SPONSORING/MONITORING AGENCY REPORT NUMBER**
11. SUPPLEMENTARY NOTES The views expressed in this thesis are those of the author and do not reflect the official policy or position of the Department of Defense or the U.S. Government.			
12a. DISTRIBUTION / AVAILABILITY STATEMENT Approved for public release; distribution is unlimited			**12b. DISTRIBUTION CODE**

13. ABSTRACT (maximum 200 words)

Spray cooling is a promising means of dissipating large steady state heat fluxes in high density power and electronic systems, such as thermophotovoltaic systems. The present study reports on the effectiveness of spray cooling in removing heat fluxes as high as 220 W/cm^2. An experiment was designed to determine how the parameters of spray volumetric flow rate and droplet size influence the heat removal capacity of such a system. A series of commercially available nozzles were used to generate full cone water spray patterns encompassing a range of volumetric flow rates (3.79 to 42.32 L/h) and droplet Sauter mean diameters (17.4 to 35.5 micrometers). The non-flooded regime of spray cooling was studied, in which liquid spreading on the heater surface following droplet impact is the key phenomenon that determines the heat transfer rate. The experimental data established a direct proportionality of the heat flux with spray flow rate, and an inverse dependence on the droplet diameter. A correlation of the data was developed to predict heat flux as a function of the studied parameters over the range of values tested in this experiment.

14. SUBJECT TERMS Spray Cooling, High Heat Flux Dissipation, Critical Heat Flux, Nucleate Boiling			**15. NUMBER OF PAGES** 79
			16. PRICE CODE
17. SECURITY CLASSIFICATION OF REPORT Unclassified	**18. SECURITY CLASSIFICATION OF THIS PAGE** Unclassified	**19. SECURITY CLASSIFICATION OF ABSTRACT** Unclassified	**20. LIMITATION OF ABSTRACT** UL

NSN 7540-01-280-5500 Standard Form 298 (Rev. 2-89)
Prescribed by ANSI Std. 239-18

THIS PAGE INTENTIONALLY LEFT BLANK

Approved for public release; distribution is unlimited

AN EXPERIMENTAL STUDY OF STEADY STATE HIGH HEAT FLUX REMOVAL USING SPRAY COOLING

James B. Fillius
Lieutenant, United States Navy
BSME, University of Maryland, 1996

Submitted in partial fulfillment of the
requirements for the degree of

MASTER OF SCIENCE IN MECHANICAL ENGINEERING

from the

NAVAL POSTGRADUATE SCHOOL
December 2004

Author: James B Fillius

Approved by: Ashok Gopinath
Thesis Advisor

Anthony J. Healey
Chairman, Department of Mechanical and Astronautical Engineering

THIS PAGE INTENTIONALLY LEFT BLANK

ABSTRACT

Spray cooling is a promising means of dissipating large steady state heat fluxes in high density power and electronic systems, such as thermophotovoltaic systems. The present study reports on the effectiveness of spray cooling in removing heat fluxes as high as 220 W/cm^2. An experiment was designed to determine how the parameters of spray volumetric flow rate and droplet size influence the heat removal capacity of such a system. A series of commercially available nozzles were used to generate full cone water spray patterns encompassing a range of volumetric flow rates (3.79 to 42.32 L/h) and droplet Sauter mean diameters (17.4 to 35.5 micrometers). The non-flooded regime of spray cooling was studied, in which liquid spreading on the heater surface following droplet impact is the key phenomenon that determines the heat transfer rate. The experimental data established a direct proportionality of the heat flux with spray flow rate, and an inverse dependence on the droplet diameter. A correlation of the data was developed to predict heat flux as a function of the studied parameters over the range of values tested in this experiment.

THIS PAGE INTENTIONALLY LEFT BLANK

TABLE OF CONTENTS

THIS PAGE INTENTIONALLY LEFT BLANK

LIST OF FIGURES

THIS PAGE INTENTIONALLY LEFT BLANK

LIST OF TABLES

THIS PAGE INTENTIONALLY LEFT BLANK

LIST OF SYMBOLS

ΔT_e	excess temperature or difference between surface and fluid saturation temperature
h	convective heat transfer coefficient, $W / m^2 K$
$q^{"}$	heat flux, W / cm^2
P_{in}	power delivered to heater element via applied voltage, W
R	equivalent electrical resistance of cartridge heaters, Ω
A	heater element cross sectional area, cm^2
k	thermal conductivity, $W / m \bullet K$
V_{rms}	root mean square voltage, V
Δx	axial spacing between thermocouple levels, cm
D_{32}	Sauter mean diameter or droplet size, μm
$\dot{V}_{spray}$	spray volumetric flow rate, cm^3 / s
A_{flux}	area flux, cm^2 / s
ΔT_{sub}	degree of subcooling
$\rho_{g,} \rho_l$	density of fluid in vapor and liquid phases, respectively, kg / m^3
h_{fg}	latent heat of vaporization, kJ / kg
$Q^{"}$	local volumetric flux, cm / s
σ	surface tension, N / m
c_{pf}	specific heat of fluid in liquid phase, $kJ / kg \bullet K$
q_{ratio}	heat flux ratio
$\dot{V}_{ratio}$	flow rate ratio
$d_{32_{ratio}}$	droplet size ratio
A_h	heater element area, cm^2
ε	wetted fraction

THIS PAGE INTENTIONALLY LEFT BLANK

ACKNOWLEDGMENTS

I would like to thank my predecessor in this work, Lieutenant Matthew Cryer, for laying the foundation of an experiment that I was able to expand upon. I want to recognize Professor Gopinath for his patience, time, and insight that greatly assisted me throughout the course of this research. I thank my wife Kimberly for her steadfast love and support that allowed me to complete this project.

THIS PAGE INTENTIONALLY LEFT BLANK

I. INTRODUCTION

The high temperature operational environment associated with many of today's industrial and technological applications has resulted in an increased demand for the development of thermophotovoltaic (TPV) technology as a means of generating power. This form of energy conversion has proven to be very efficient with the potential for high power density generation in excess of 100 W/cm^2 through the use of micro-thermophotovoltaic (MPTV) systems. As is the case with any innovative technology, an increased understanding of all components of this technology will be necessary before it can be considered a viable alternative for any existing form of high power density generation.

An MPTV system typically consists of a heat source, an emitter that transfers the energy of the heat source via radiation, a semiconductor receiver in close proximity to the emitter which converts the thermal photonic energy to useful electrical current, and an electrical distribution system (Cryer, 2003). The present study will focus on the large amount of radiated energy produced by the emitter and dissipated as waste heat in the semiconductor receiver that must be rejected to ensure operation within safe temperature parameters.

In recent years there has been an increase in the demand for new techniques capable of removing high heat fluxes. These demands come from a variety of industrial and technical sources including the electronics industry where excessive temperatures can lead to failure in microelectronic devices, the metallurgical industry where high heat flux removal is necessary to maintain material properties during casting and quenching processes, and optical applications where laser diodes capable of high heat flux dissipation require heat flux removal to ensure proper operation (Ortiz et al., 1999). An MPTV system is capable of generating waste heat in excess of 100 W/cm^2. Due to the constraints imposed by conventional cooling techniques such as forced convection, phase change heat transfer is the most realistic means of removing heat fluxes of this magnitude. Phase change heat transfer is characterized by high heat fluxes for relatively small temperature differential between the heated surface and heat transfer fluid. High

heat flux cooling techniques that utilize phase change heat transfer include: jet impingement cooling, forced convection cooling, and spray cooling (Sehemby et al., 1994). Spray cooling is regarded as the most effective phase change cooling technique resulting in the highest heat fluxes. This can be attributed to the directness contact between the heat transfer fluid and heated surface. Results of various phase change cooling techniques are summarized in Table 1(Xia, 2002). The critical heat flux (CHF) parameter used in Table 1 is the heat flux associated with the temperature difference between the heated surface and saturation temperature such that increasing the heated surface temperature would result in a decrease in heat flux. Operating a heat transfer surface above the CHF could result in its destruction or failure, therefore it is feasible to operate near this point, but not recommended to operate above it.

Cooling Scheme	CHF (W/cm^2)	ΔT
Spray Cooling	600	Small
Jet Boiling (macro-surface)	100-300	Large
Jet Boiling (micro-surface)	500	Large
Subcooilng	500	Large
Convective Boiling (mini-channel)	200	Large
Convective Boiling (micro-channel)	300	Large
Pool Boiling	100	Large

Table 1. Critical Heat Flux and Temperature Rise in Phase Change Cooling Techniques

Spray cooling involves spraying a heated surface with a liquid that is subcooled or at its saturation temperature. The small liquid droplets, with mean diameters on the order of microns, impact the heated surface and form a liquid film. Spray generators can be classified into two separate categories: pressure atomizers or nozzles, and gas-assisted atomizers. A pressure nozzle is the more simplified of the two methods as it uses a single working fluid. Alternatively, gas-assisted atomizers, also called air-atomizers, require the use of a secondary gas to break the liquid into fine droplets. Air atomizers are capable of producing smaller droplet sizes and larger heat fluxes than pressure nozzles, but the presence of a non-condensable secondary gas in a phase change heat transfer process is undesirable.

The present study is an experimental investigation of pressurized spray cooling using commercially available nozzles and fluid delivery system. The goal of the investigation is to provide an understanding of the practicality of using spray cooling to

remove waste heat generated by an MPTV system, through the use of a simple model under a variety of mass flow rates and spray droplet diameters.

A. PREVIOUS WORK

There are numerous references in the literature that investigate spray cooling as a method for high heat flux dissipation. The six primary parameters that affect spray cooling effectiveness found in the literature are: droplet size (Schmidt,[2001], Toda [1971], Liu [2001], Webb et al. [1992], Choi et al. [1986], Estes et al.[1994], Cryer [2003]), mass flow rate (Xia [2002], Ortiz et al. [1999], Halvorson et al. [1994], Liu [2001], Webb et al. [1992], Choi et al. [1986], Cryer [2003]), surface roughness (Bernardin et al. [1997], Mesler [1993], Ortiz et al. [1999], Pais et al. [1992]), impact angle (Ortiz et al. [1999], Estes et al. [1994]), degree of sub-cooling (Ortiz et al. [1999], Estes et al. [1994]), and reduced system pressure (Marcos, 2002). The majority of these experiments studied the effects of these parameters on the heat flux removal capacity using spray cooling under transient conditions. The most extensive experiment found in the literature by (Ortiz et al., 1999) studied the effect of mass flow rate, impact angle, surface roughness, and the degree of sub-cooling under steady state conditions. Cryer (2003) conducted a spray cooling experiment on the effect of mass flow rate and droplet size on power density removal using full cone pressure nozzles. The present study is an expansion of Cryer's work. A summary of the previous spray cooling experimentation and the present work is included in Table 2. A selected number of these experiments are discussed in further detail in the discussion of the experimental results.

Author	Droplet Diameter	Nozzle Type	Mass Flow Rate, L/h
Gaugler [1966]	128-250 μm	full cone	0.86
Choi et al. [1986]	0.43-0.56 mm	piezo-electric	not available
Marcos et al. [2002]	not available	full cone	0.17-0.50
Webb et al. [1992]	32-56 μm	full cone	6
Pais et al. [1992]	7-28 μm	air assisted	1.0-5.0
Liu [2001]	12-198 μm	air assisted	not available
Toda [1971]	88-146 μm	air assisted	2.92
Halvorson et al. [1994]	2.8-3.8 mm	17-22 gauge needle	0.07
Ortiz et al. [1999]	85-100 μm	full cone	1.48-2.91
Xia [2002]	132 μm	piezo-electric	not available
Estes et al. [1994]	110-225 μm	full cone	not available
Cryer [2003]	19-32 μm	full cone	1.96-9.66
Fillius [2004]	17-35 μm	full cone	3.78-42.32

Table 2. Summary of Present and Previous Work

B. THE BOILING PROCESS

Spray cooling utilizes phase change heat transfer resulting in high heat transfer rates for relatively low superheats or excess temperatures. These terms can be used interchangeably to describe the difference in temperature between the heated surface to be cooled and the cooling fluid. When the temperature of the hot surface is greater than the saturation temperature of the cooling fluid a phase change occurs at the solid-liquid interface and boiling takes occurs. In these cases of phase change heat transfer the associated latent heat is a significant, but not lone contributor to the overall heat transfer rate. In addition to the latent heat contribution, the surface tension between the liquid-vapor interface and the buoyancy force attributed to the density difference between the two phases account for higher heat transfer coefficients and resulting heat transfer rates than those associated with other non-phase change convective heat transfer processes.

Nukiyama's boiling curve can be effectively utilized to identify and explain the various boiling regimes. Incopera et al. (1990) used this curve to present a thorough discussion of the boiling process, particularly in the nucleate regime. Nukiyama generated this curve by measuring the heat flux from a nichrome wire heated by electrical current to saturated water. A derivative of Nukiyama's boiling curve is shown in Figure 1. The value on the abscissa is the excess temperature, ΔT_e, or the difference in temperature between the surface temperature of the wire and the saturation temperature of the water. The ordinate value is the measured heat flux.

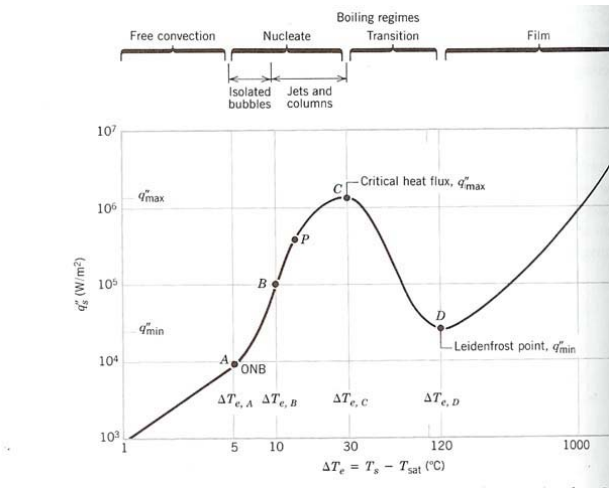

Figure 1. Typical Boiling Curve for Water at 1atm (Incropera et al., 1990)

The first region of interest occurs from the inception of the curve until point A is reached. This region is associated with free convection boiling and is typical for $\Delta T_e \leq 5^\circ \mathrm{C}$. Boiling at the saturation temperature is not promoted under these conditions due to the insufficient amount of vapor in contact with the liquid phase, thus fluid motion can be primarily attributed to free convection.

Point A is also associated with the onset of nucleate boiling, ONB, where bubble inception occurs. The region ranging from points A-C is termed nucleate boiling and is the region in which spray cooling is most effective. The nucleate boiling regime exists in the approximate excess temperature range spanning from $5^\circ \mathrm{C} \leq \Delta T_e \leq 30^\circ C$. In region A-B isolated bubbles begin to form and then separate from the surface, resulting in markedly increased values of the convective heat transfer coefficient, h, and the heat flux, q_s" due to substantial fluid mixing near the surface. The heat transfer in this region is credited to the direct transfer from the surface to the liquid in motion at the surface. When ΔT_e is increased beyond the excess temperature associated with point B, the number of bubble nucleation sites increases resulting in increased bubble formation. The increase in bubble formation results in interference and coalescence between bubbles.

The inflection point shown as point P in Figure 1 represents a point where the heat transfer coefficient reaches a maximum value. This point warrants consideration due to the fact that the heat transfer coefficient decreases while the heat flux increases

with an increase in excess temperature. The heat flux, the product of h and ΔT_e, increases because the increase in ΔT_e exceeds the corresponding reduction in h. This trend continues until point C is reached and the increase in ΔT_e is balanced by the decrease in h. At this point the critical heat flux, or maximum value of heat flux, is achieved. The critical heat flux in water spray cooling exceeds 1 MW/m^2. At the critical heat flux vapor leaves the surface at such a high rate that it is difficult to continuously wet the surface with liquid. Critical heat flux can be considered a function of vapor production where a suppression of the liquid supply to the heat transfer surface is generated by the presence of bubbles produced within the liquid film that is formed on the heated surface (Pais et al.,1994). Operating at or near this value results in optimal heat transfer, but operating a heat transfer surface beyond this point could result in an inability to wet the surface sufficiently and in potential damage to the system.

Transition boiling occurs in the region from points C to D in Figure 1 where $30^\circ \mathrm{C} \le \Delta T_e \le 120^\circ C$. Heat transfer during this range of excess temperature is characterized by rapid bubble formation that results in the development of a vapor blanket on the surface. In this region both h and q_s" decrease as ΔT_e increases due to thermal conductivity of this vapor being significantly lower than that of the cooling liquid.

At point D in Figure 1, q_s" is at a minimum point referred to as the Leidenfrost point. The Leidenfrost point represents the onset of film boiling and occurs at ΔT_e values in excess of 120°C. At this point the vapor blanket that began forming on the surface during transition boiling now completely covers the surface with heat transfer from the surface to the liquid via conduction through the vapor blanket.

C. SPRAY COOLING PHYSICS

Figure 2 illustrates the spray cooling process with a heated surface being sprayed with a saturated liquid. Once the impinging spray droplets make contact with the heated surface they form thin discs whose interactions result in the formation of a thin liquid film.

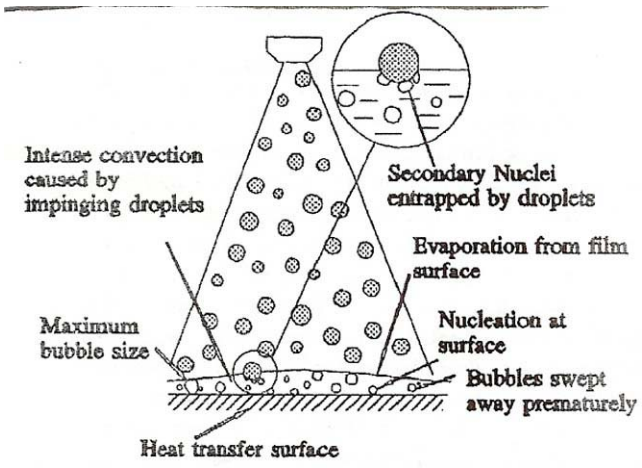

Figure 2. Spray Cooling Physics (Pais et al., 1994)

As the drops of the cooling spray continuously wet the surface mixing ensues and contributes to an increase in the thermal conductivity of the liquid film. Evaporation takes place from the free surface of the liquid film as hot liquid is displaced from the heater surface to the liquid film surface.

In addition to the evaporation that occurs from the liquid film surface, the presence of boiling within the liquid form is an important contributor to the heat transfer coefficient. Nucleate boiling exists in the liquid film and the presence of bubbles can be observed. The origin of these bubble nuclei in the majority of boiling cases can be solely attributed to the cavities on the heater surface with trapped vapor (Rosenhow,1985). In the case of boiling in thin liquid films a second source exists for bubble nucleation. This second source is termed secondary nucleation (Mesler, 1992). As a bubble reaches the liquid surface and bursts, the upper surface of the bubble collapses resulting in small droplets which then rain back on the liquid surface. These droplets entrain small amounts of vapor into the liquid film in the form of small vapor bubbles. These small vapor bubbles can get in close proximity to the heated surface and act as nuclei for more boiling. This process is secondary nucleation.

Figure 2 shows that during spray cooling the sources for secondary nucleation are the spray droplets themselves. Nucleate boiling in spray cooling requires very little assistance from the aforementioned surface cavities, but when the required superheat is reached the surface cavities must be active. Although the contribution of surface cavities

is limited a distinction between nucleate boiling due to surface cavities and nucleate boiling due to secondary nuclei is warranted. As illustrated in Figure 2, as the liquid film surface is impinged upon with a high velocity of spray droplets, the bubbles being formed within the film will most likely not survive once their size reaches the thickness of the liquid film. As a result, the bubbles can prematurely break down before the free surface of the liquid film, or microlayer, is even evaporated (Cooper, 1966). This premature bubble breakdown has the effect of increasing bubble formation. Since heat transfer due to bubble growth is at a maximum at the early stage of bubble growth where microlayer evaporation is dominant, this increase in bubble frequency results in a marked increase in the average heat transfer coefficient. In effect, the premature bubble breakup increases the net time in which microlayer evaporation exists on the surface increasing the heat transfer coefficient. This only occurs for bubbles formed at surface cavities since those formed due to secondary nucleation will never get close enough to the surface of the liquid film for microlayer evaporation to occur.

This theoretical development suggests that there are three components to spray cooling heat transfer: forced convection with surface evaporation, nucleate boiling from surface cavities, and nucleate boiling due to the contribution of secondary nuclei.

II. EXPERIMENTAL SETUP

A. SPRAY DELIVERY SYSTEM

The spray delivery system is shown schematically in Figure 3 and photographically in Figure 4. The delivery system consists of a pressurized nitrogen cylinder connected to a liquid pressure vessel containing distilled water. Distilled water was selected as the working fluid to eliminate any chance of impurities or particulate matter that might erroneously affect the heat transfer properties of the fluid or system or adversely affect the performance of the mini nozzles. The working fluid was transferred from the pressure vessel to the nozzle via ¼" stainless steel tubing connected with Swagelock compression fittings. The stainless steel tubing was instrumented with a pressure gage and inline type E thermocouple probe to monitor distilled water temperature.

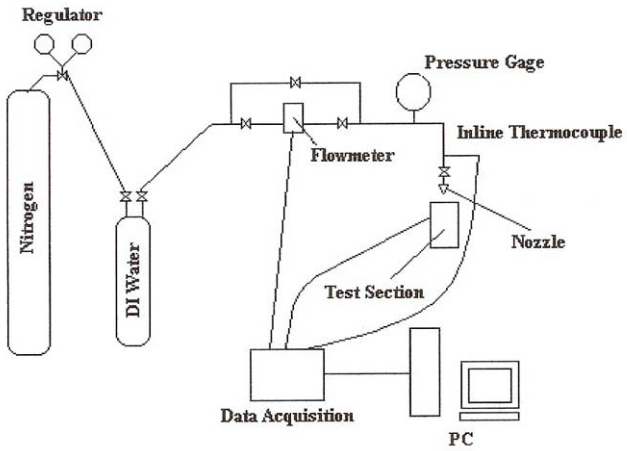

Figure 3. Spray Delivery System Schematic (Cryer, 2003)

Figure 4. Spray Delivery System

A typical nozzle is illustrated in Figure 5. The nozzles used were Hago M-Type full cone mini-nozzles with an 80 degree spray angle. The manufacturer reported droplet sizes ranging from 17.4 to 35.5 μm at pressure set points ranging from 100 to 500 psi . The droplet sizes reported by the manufacturer are the Sauter mean diameter (SMD) and are determined using a MUNHILL PSA-32 particle analyzer which measures droplet sizes based on Fraunhofer's Diffraction Principle. The Sauter mean diameter is the diameter of hypothetical spray droplet whose ratio of volume to surface area is equal to the ratio of volume to surface area for that of the entire spray. The SMD's were verified by Hago Precision Nozzles using a photomask test reticle containing a known distribution of droplets per ASTM draft photomask/reticle method. No independent tests were conducted to verify the manufacturer's SMD data. The manufacturer reported flow rates ranging from 3.79 to 42.32 L/hr for the same range of operational pressures which were verified experimentally using a stop watch and graduated cylinder.

Figure 5. Typical Nozzle-Hago 'M' Series Mini-Nozzle

B. HEATER ELEMENT

The heater element consists of a 5.5"long copper cylinder with a base diameter of 2.5" tapered to a reduced diameter of 1.25" at the uppermost portion. The reduction in diameter resulted in an increase in heat flux at the tip of the copper cylinder. At the reduced diameter section of the heater element thermocouple holes were drilled at three different axial levels spaced at 0.125" intervals to facilitate the determination of the heat flux. Two additional holes at each of these three axial positions were then drilled 120 degrees apart in the circumferential direction resulting in a total of nine thermocouple holes. A schematic of the heater block and thermocouple placement is illustrated in Figure 6. Nine type E thermocouples were inserted into the holes drilled into the reduced diameter portion of the heater element at a depth of 0.5". The thermocouples located at the same axial level, but separated by 120 degrees were used to verify the assumption of one-dimensional heat conduction on the axial direction.

The element was heated by four Watlow 1000 Watt (nominal) cartridge heaters that were fitted into the 2.5" diameter base of the cylindrical heater element using a thermal epoxy. The heaters were fitted in place with the epoxy to eliminate all air gaps and facilitate the best path for heat conduction. These heaters are shown in Figure 7. The heaters were arranged in a series-parallel connection providing an equivalent

resistance of 13.94 Ω. Power was provided to the cartridge heaters via a Staco variable transformer that provided a variable voltage ranging from 0 to 167.58 V_{rms}. The test section was placed in PVC tube insulated on all but the top surface to ensure one dimensional heat transfer in the axial direction of the cylinder by minimizing heat loss in the radial direction. Figure 8 shows a photograph of the heater element prior to instrumentation with thermocouples and cartridge heaters. Figure 9 shows the base of the heater element with four cylindrical holes for cartridge heater placement, and Figure 10 shows a photograph of the cartridge heaters fitted into the base of the heater element. Figure 11 is a photograph of the instrumented heater element and cartridge heaters housed in the insulated PVC tube as oriented prior to the commencement of spraying.

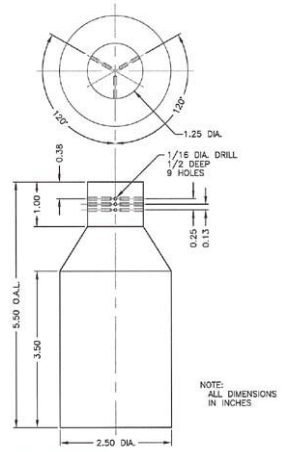

Figure 6. Heater Element Schematic

Figure 7. Cartridge Heaters

Figure 8. Heater Element


Figure 9. Heater Element Base

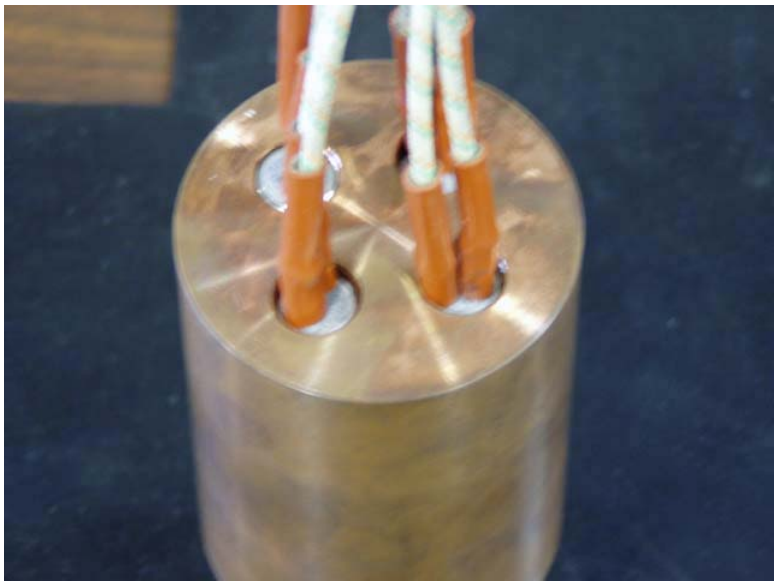

Figure 10. Cartridge Heater Placement

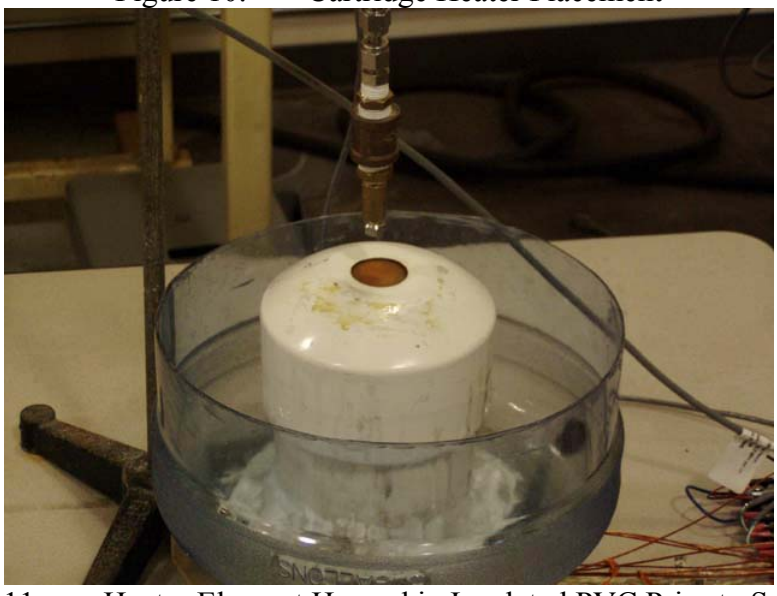

Figure 11. Heater Element Housed in Insulated PVC Prior to Spraying

C. INSTRUMENTATION AND DATA ACQUISITION

The thermocouple and pressure gage output was connected to an HP 3852 data acquisition unit. The data acquisition unit was connected to a personal computer running an installed version of Lab View software. The 1.25" diameter portion of the heater element was instrumented with a total of nine type E thermocouples. The thermocouples were oriented vertically in groups of three at 0.125" intervals in the axial direction and 120 degree intervals in the circumferential direction. This orientation allowed for the calculation of the one-dimensional heat flux in the axial direction and ensured that the

axial temperature at a given location was uniform at that given axial location along any point of the copper cylinder's circumference. The thermocouples were affixed to both the heater element using thermal epoxy. A single type E thermocouple was employed to monitor the distilled water temperature used in spray cooling the heater element surface. This resulted in a total of 10 thermocouple channels whose outputs were displayed in the Lab View program.

THIS PAGE INTENTIONALLY LEFT BLANK

III. EXPERIMENTAL PROCEDURE

A. CALIBRATION AND UNCERTAINTY ANALYSIS

The primary variable observed during this experiment was the temperature of the heated surface . The heat flux dissipated heated surface was calculated using these temperature readings and which were monitored on a real time basis. The experimental heat flux was calculated using the temperature difference between the three levels of thermocouples in the reduced area section of the copper heater element assuming one-dimensional conductive heat transfer and applying Fourier's Law:

$$q'' = k\frac{\Delta T}{\Delta x} \tag{1}$$

where ΔT is the temperature difference between thermocouple levels, Δx is the distance between thermocouples, and k is the thermal conductivity of copper taken to be 4.01 W/cm/K.

The uncertainty in the measured heat flux is dependant upon ΔT and was calculated using:

$$\varepsilon_q = q''\bullet\left[\left(\frac{\varepsilon_x}{\Delta x}\right)^2 + \left(\frac{\varepsilon_T}{\Delta T}\right)^2\right]^{\frac{1}{2}} \tag{2}$$

where ε_T and ε_x are the uncertainty in the temperature and the distance measured between thermocouples, respectively. Values from the manufacturer indicate an error for E-type thermocouples to be $\pm 0.5^{\circ} C$ and the uncertainty in the thermocouple spacing was taken as ±0.00005 m. These values provided an uncertainty in the heat flux measurements of less than 7%.

The uncertainty associated with the volumetric flow rate of the impinging spray can be attributed to the fluctuations in pressure observed during testing. These fluctuations ranged from +/- 15 psi at low pressure set points (i.e. 100 psi) and +/-3 psi at higher pressure set points (i.e. 500 psi). The uncertainty can be expressed mathematically

$$\Delta V_{spray} = \frac{\delta \dot{V}}{\delta p} \bullet |\Delta p| \tag{3}$$

where the derivative term is determined from the logarithmic fit equation to flow rate-pressure relationship obtained from the given nozzle data, and the absolute value term is the observed experimental pressure fluctuations. The largest pressure fluctuations occurred at the lowest pressure settings or lowest flow rates, while the smallest fluctuations took place at the highest pressure settings corresponding to the largest flow rates. For this reason the volumetric flow rate uncertainty is expressed in the range of 2.8-71.3 percent. The largest uncertainties occurred at the lowest pressures (lowest flow rates) where the set point was difficult to maintain and the largest, most frequent pressure fluctuations occurred.

It was possible to predict the input flux to the heater via the variable voltage transformer and the series-parallel configured cartridge heaters. The resistance of each cartridge heaters was measured using a digital multi-meter and then an equivalent resistance was calculated using appropriate parallel and series resistance equations. The applied voltage generated by the variable voltage transformer was monitored using a digital multi-meter such that the input power could be calculated using:

$$P_{in} = \frac{V_{rms}^{\ 2}}{R} \tag{3}$$

where V_{rms} is the output root mean square voltage delivered to the cartridge heaters, and R is the equivalent resistance of the series-parallel arranged cartridge heaters. The input flux could then be calculated using the calculated input power and the area of the copper heater element determined using the formula for an area of a circular cross section. The input flux was then determined using:

$$q_{in} = \frac{P_{in}}{A} \tag{4}$$

where P_{in} is the calculated input power and A is the area of the circular cross section whose surface is subjected to the cooling spray. This preliminary calculation provided a check against the experimentally determined heat flux based on the heater element

temperature gradients from equation (1). The experimental heat flux value should be equal to or slightly less than the predicted heat flux due to minimal losses. The small variation in temperature between the three circumferentially spaced thermocouples at each axial location verified the assumption of one-dimensional heat conduction in the axial direction.

B. PROCEDURE

The procedure used in this experiment was determined by considering the requirements for steady state one-dimensional heat transfer. Two independent variables were studied: spray mass flow rate and spray droplet size. The mass flow rates and droplet sizes were provided by the manufacturer for operating pressures values of 100, 200 300, and 500 psi. Both droplet sizes and flow rates at pressures not provided by the manufacturer were determined by using a logarithmic extrapolation from the provided data. One such logarithmic fit for droplet size versus operating pressure is shown in Figure 12. The corresponding logarithmic fit for flow rate versus operating pressure for the same nozzle is shown in Figure 13.

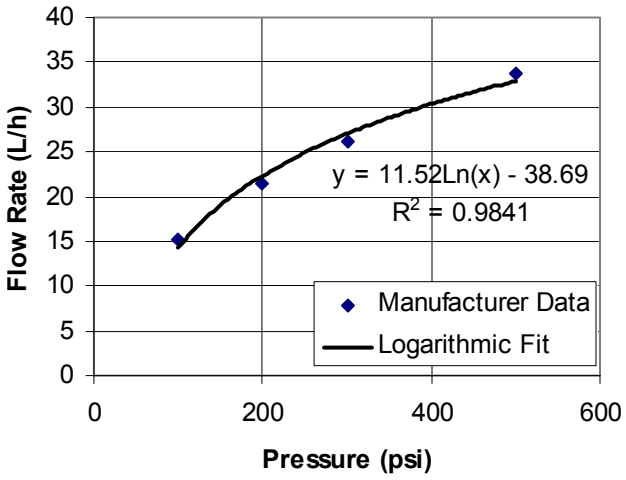

Figure 12. Logarithmic Fit for Flow Rate versus Pressure for M4 Nozzle

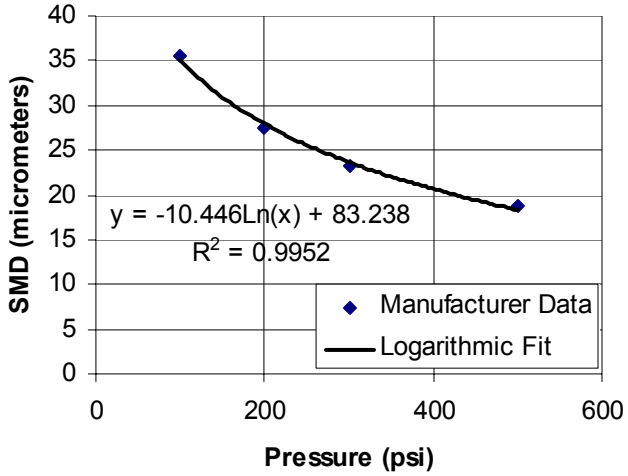

Figure 13. Logarithmic Fit for Droplet Size versus Pressure for M4 Nozzle

The mass flow rate and corresponding droplet size for each nozzle was controlled through the use of a throttle valve to arrive at a pressure set point for each nozzle. The throttle valve was adjusted until the pressure set point was reached and both the mass flow rate and droplet size was determined using the provided manufacturer data supplemented with the logarithmically fitted data. Five operational pressure set points were chosen ranging from 100-500 psi, in 100 psi increments. Five different nozzles were tested at these five pressure set points generating twenty-five sets of data. The corresponding droplet sizes and mass flow rates for each nozzle at the pressure set points are shown in Table 3 and Table 4, respectively.

Nozzle Pressure	M1	M2	M3	M4	M5
100	28.4	30.3	32.4	35.5	33.7
200	22.6	25.8	25.5	27.5	29.3
300	20.7	21.7	22.4	23.2	24.6
400	18.7	20.3	19.9	20.7	21.9
500	17.4	18.7	18.3	18.8	19.3

Table 3. Nozzle Droplet Sizes (micrometers) at Operational Pressures

Nozzle Pressure	M1	M2	M3	M4	M5
100	3.79	7.57	11.36	15.14	18.93
200	5.34	10.71	16.05	21.42	26.76
300	6.55	13.09	19.68	26.23	32.79
400	7.58	15.16	22.76	30.33	37.92
500	8.47	16.92	25.4	33.84	42.32

Table 4. Nozzle Mass Flow Rates (L/h) at Operational Pressures

Prior to testing each nozzle the heater element surface was cleaned with alcohol and polished with 140, 150, and 220 grit grinding paper in progression to ensure a consistently clean and rough spray surface, free of any particulates or oxidation. The spray nozzle was installed at a distance of 0.75" from the heater element surface to allow for complete spray coverage of the heated surface at a level 90 degree spray angle. This distance was calculated using simple trigonometry based upon the known cone angle of the spray nozzle and the measured diameter of the heater element being sprayed.

Once the nozzle under consideration was in place the spray delivery system was aligned such that spraying could commence with the turning of a single valve. The heater element was brought up to temperature slowly by increasing the voltage supplied to the heaters via the variable voltage controller in 5 V increments. Spray flow was initiated at an operating pressure of 100 psi when the surface temperature of the heater element was estimated to be $95^{\circ}C$. This temperature was estimated based upon the known input voltage and corresponding input heat flux along with the required temperature difference between the surface and the first thermocouple location to achieve that flux. The voltage was then again increased incrementally in an effort to achieve a steady state surface temperature in the $105-110^{\circ}C$ range while in the presence of the cooling spray. Steady state was defined as the condition when temperatures did not change throughout the course of a three-minute period. At this point data was collected before increasing the pressure to the next highest set point for that particular nozzle. After steady state conditions were achieved and data was collected for the 500 psi pressure set point the cartridge heaters were de-energized, the next nozzle was installed, and the heater element was permitted to cool to ambient temperature prior to testing the next nozzle.

The $105-110^{\circ}C$ surface temperature that was selected to define steady state conditions was based upon the motivation to safely operate within the nucleate boiling regime while keeping in mind the upper end of that regime coincides with the critical heat flux. Although a higher surface temperature in closer proximity to the critical heat flux would have resulted in better spray cooling conditions and thus and higher heat flux dissipation rates, the lower surface temperatures allowed for both effective two phase cooling and component operating temperatures that would not result in system burnout.

The temperature distribution for the M2 nozzle at 400 psi is shown below in Figure 14. Temperatures T1-T3 represent the temperatures in the uppermost axial location from the heater element surface separated by 120 degrees, T4-T6 are the thermocouples at an axial location 0.125" below the first three, and T7-T9 represent the lowest axial level of thermocouples in closest proximity to the cartridge heaters, but 0.63" from the surface of the heater element subject to cooling spray. As expected the lowest temperatures occur at the thermocouple levels closest to the surface, i.e. T1-T3, and the highest are at the location closest to the cartridge heaters, i.e. T7-T9. The flat temperature profile and the fact that the temperatures for each group deviate by no more than $1.5^{\circ}C$ suggest that the assumption of steady state one-dimensional conduction heat transfer in the axial direction is valid.

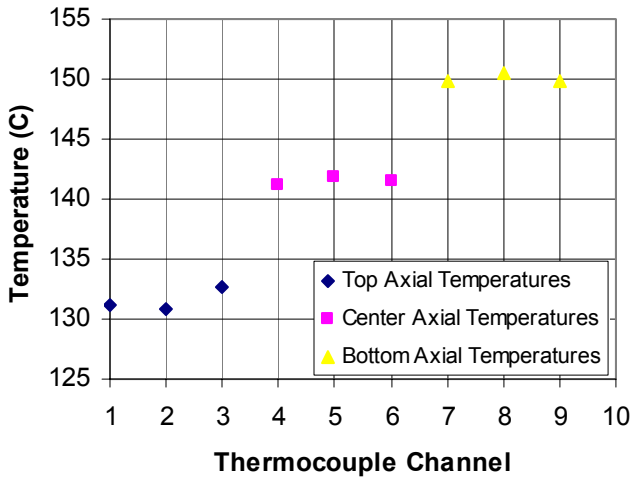

Figure 14. Steady State Temperature Distribution for M2 Nozzle at 400 psi

The experimental heat flux was determined using (1) where k is the thermal conductivity of copper, Δx is the axial spacing between the T1-T3 and T7-T9 level of thermocouples, and ΔT is defined as the difference between the average value of temperature between these respective levels:

$$\Delta T = \left(\frac{T7+T8+T9}{3}\right) - \left(\frac{T1+T2+T3}{3}\right) \tag{5}$$

THIS PAGE INTENTIONALLY LEFT BLANK

IV. RESULTS AND DISCUSSION

The experimental procedure outlined in Tables 3 and 4 resulted in twenty-five sets of data for the purpose of studying dissipated heat flux as a function of the variation of two independent parameters: spray volumetric flow rate and droplet size. The results and subsequent discussion will be presented separately for each of these parameters.

A. SPRAY VOLUMETRIC FLOW RATE

The effect of the variation of the volumetric flow rate of the cooling spray on dissipated heat flux is summarized in Figure 15 for the entire range of experimental flow rates (3.79 to 42.32 L/hr). It is important to note that the data is presented on a per nozzle basis and the general trend is clear that the capacity for heat flux dissipation increases with increasing flow rate for all nozzles under consideration.

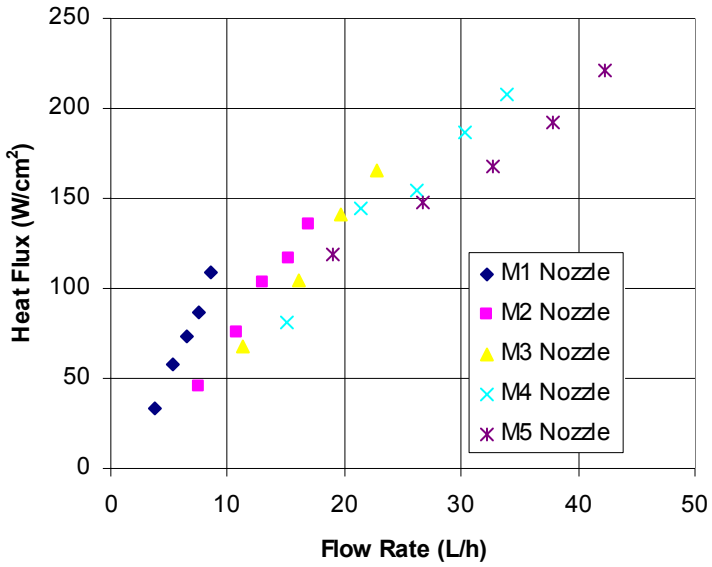

Figure 15. Heat Flux Dissipated versus Flow Rate

The highest experimental flow rate of 42.32L/h resulted in 221.2 W/cm^2 of dissipated heat, which was also the highest value heat flux achieved in the experiment.

This general trend of increasing heat flux dissipation with increasing volumetric flow rate was also seen in Cryer's experimental data. Cryer utilized the Hago B series nozzles which delivered flow rates from 2.05 to 9.68 L/h, resulting in a maximum heat flux dissipation of 56.5 W/cm^2. These results are shown in Figure 16.

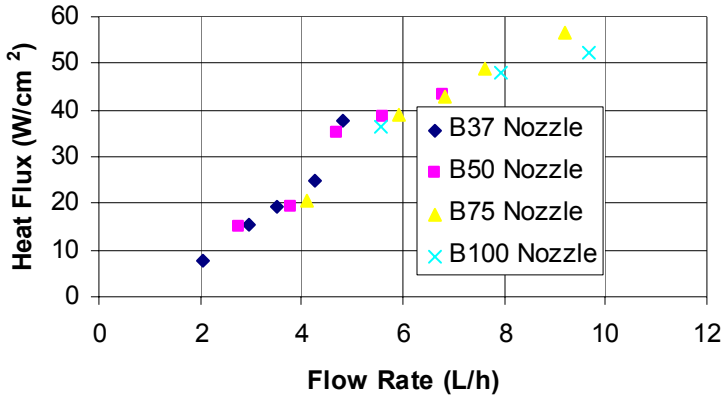

Figure 16. Heat Flux Dissipated versus Flow Rate (Cryer, 2003)

The relationship between flow rate and dissipated heat flux is further emphasized by looking at the relationship between the two while keeping the parameter of droplet size constant. Figure 17 shows five sets of data where either two or three different flow rates had corresponding SMD values that were within 0.4 micrometers of each other.

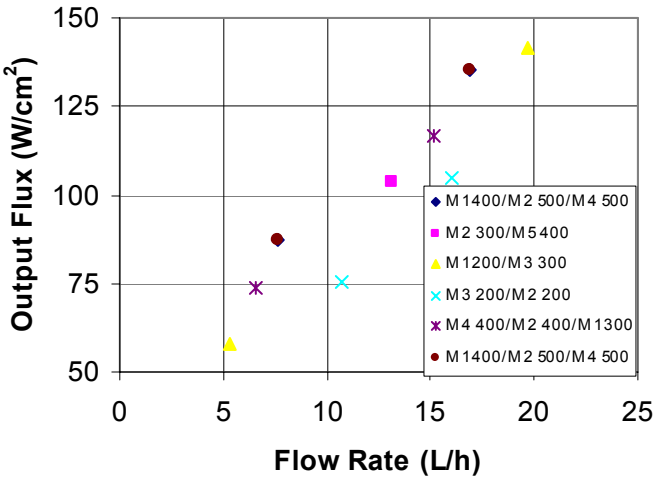

Figure 17. Heat Flux Dissipated versus Flow Rate at Constant SMD

During spray cooling of a heat transfer surface at surface temperatures greater than the liquid heat of vaporization water is continuously evaporated from the liquid film surface. High flow rate sprays, or high-density sprays, continuously flood the surface with fluid and replace the water that is evaporated in the liquid film (Sehmbey et al., 1994). Secondary nucleation is the result of the entrapment of vapor bubbles by impinging spray cooling droplets within the liquid film. High spray flow rates enhance secondary nucleation as it permits bubbles to get in close enough proximity to the heat transfer surface to allow microlayer evaporation (Ortiz, 1999). Multiple spray cooling studies have also shown that heat flux increases with increasing volumetric or mass flow rate of the spray to include: Pais et al. (1992), Ortiz et al. (1999), Liu (2002), Halvorson et al. (1994), Sehmbey et al. (1995), Choi et al. (1986), and Cryer (2003).

B. SPRAY DROPLET DIAMETER

The droplet diameters in this experiment were classified as the Sauter mean diameter (SMD) or D_{32}. The SMD is defined as the diameter of the drop with a volume to surface area ratio that is equal to the volume to surface area ratio of the entire spray

(Estes, 1996). The experimental data encompasses SMD values ranging from 17.4 to 35.5 micrometers. Figure 18 shows the spray cooling heat removal capacity of the system against the droplet diameter on a per nozzle basis.

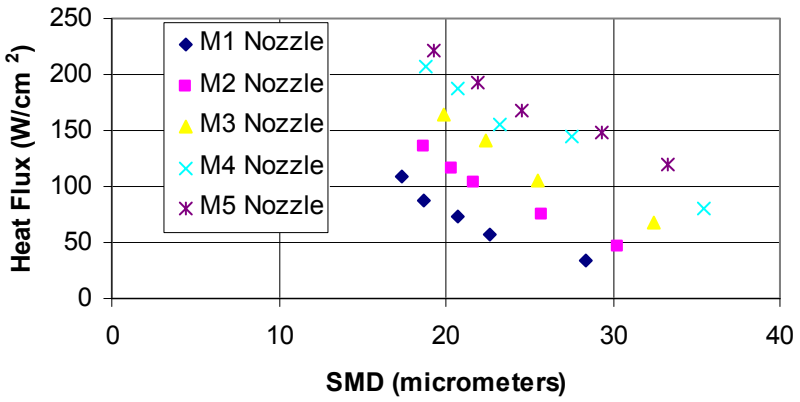

Figure 18. Heat Flux Dissipated versus SMD

For the case of each nozzle tested, heat removal increased with decreasing droplet sizes. Cryer's data representing a range of droplet diameters from 19-32 micrometers shows a similar trend between heat flux dissipation and SMD. This data is represented in Figure 19.

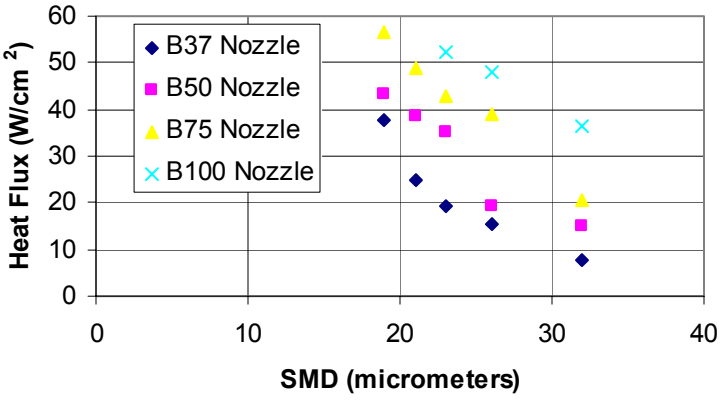

Figure 19. Heat Flux Dissipated versus SMD (Cryer, 2003)

This trend of increasing heat flux dissipation with decreasing droplet sizes can also can be demonstrated by studying the effect for the case of constant flow rates for varying droplet sizes. The data represented in Figure 20 is an effort to demonstrate the relationship between heat flux and SMD for cases of constant flow rates. It encompasses six sets of data comprised of five pairs and one trio of flow rates and corresponding SMD's where no flow rates within a single grouping deviate more than 0.8L/h.

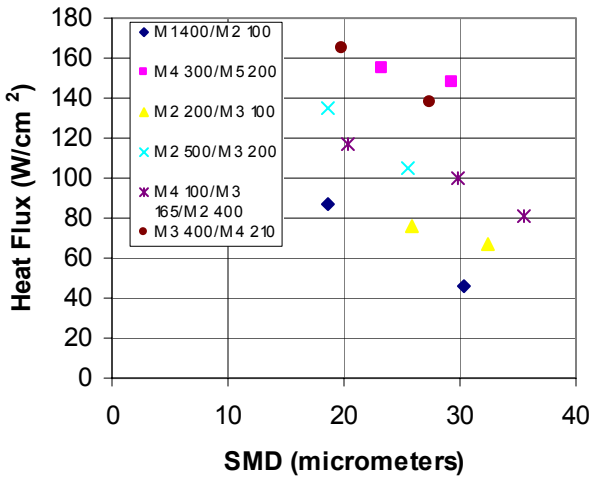

Figure 20. Heat Flux Dissipated versus SMD for Constant Flow Rates

The data shows that for a constant volumetric flow rate the dissipated heat flux increases with a decreasing value of SMD. Pais et al. (1994) showed that the increase in SMD results in a decrease in the heat transfer coefficient and the corresponding heat flux. Sehmbey et al. (1994) took this a step further and suggested that heat flux varies as $SMD^{-0.24}$. This phenomenon can be explained by examining the definition of the Sauter mean diameter mathematically.

$$D_{32} = \frac{V_{spray}}{A_{spray}} = \frac{\Pi D_{32}^{\,2}/6}{\Pi D_{32}^{\,2}} = \frac{D_{32}}{6} \tag{6}$$

Upon examining the above equation it can be seen that for a given flow rate, a smaller droplet diameter results in a larger overall spray surface area consisting of a

larger quantity of smaller diameter individual droplets. Conversely, for a fixed flow rate, a larger diameter droplet would result in less surface area coverage of the heat transfer surface by the impinging spray adversely affecting the heat removal capacity.

C. SYSTEM LOSSES

Heat flux values in excess of 220 W/cm^2 were removed from the system during this experiment by utilizing spray cooling techniques. The system was heated with an input voltage via embedded cartridge heaters in the base of the heater element, but spray cooling occurred at the non-insulated surface of the element located at a distance from these heaters. The extracted heat flux as a result of spray cooling ranged from 87 to 92 percent of the heat flux delivered to the system via the input voltage across the heaters. A comparison between the input and output flux for the M2 nozzle over its range of operating pressures is shown as Figure 21.

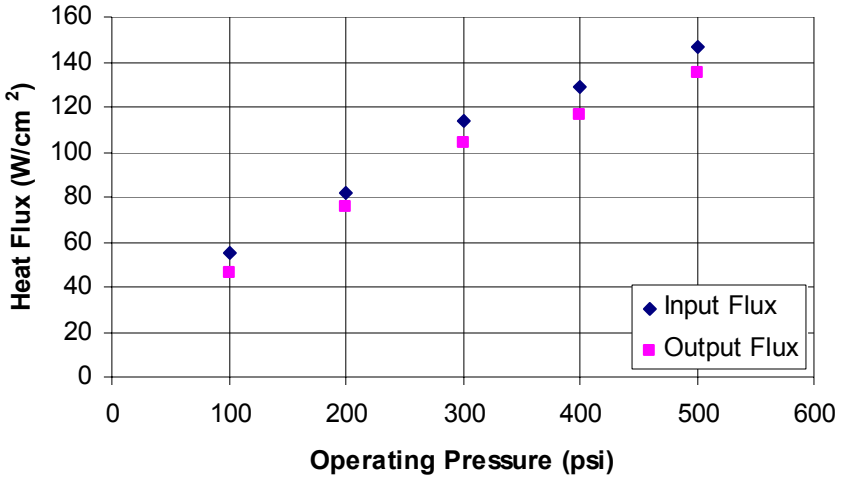

Figure 21. Comparison of Input and Output Flux for M2 Nozzle

There are several reasons for the differences that occurred between values of the input and output flux. The three axial levels of thermocouples spaced circumferentially around the heater element showed experimental temperatures that were consistent with the assumption of one-dimensional heat conduction. There were however, small differences between these circumferential temperatures at a given axial location suggesting that the heat transfer was not entirely one-dimensional. The heater element with the exception of the heat transfer surface was insulated within a PVC enclosure.

The insulation was effective during the experiment, but losses through the insulation and PVC did occur.

The hot surface of the heater element subjected to spray cooling not only exchanged heat with the cooling spray, but also with the ambient atmosphere of the testing environment. These losses can be estimated by considering the ambient air flow over the heated surface of the heater element to be free convection over a flat horizontal plate. The correlation for average Nusselt Number for the upper surface of a horizontal heated plate is given by:

$$\bar{Nu}_L = 0.54 Ra_L^{0.25} \tag{7}$$

where Ra_L is the calculated Rayleigh number. After determining the average Nusselt number one can then obtain the average convective heat transfer coefficient, and ultimately the convective heat transfer rate based on the temperature difference between the heated surface and the ambient air. Based on these assumptions, the heat loss due to free convection between the heater element surface and the ambient air was estimated to be 0.5 W/cm^2. Based on the fact that the dissipated heat flux values were in some cases in excess of 200 W/cm^2, this can be characterized as a minor system loss.

D. RESULTS PARAMETRIZATION

Liu (2002) and Cryer (2003) parameterized droplet size and volumetric flux data in terms of what was termed the area flux, A_{flux}. This was done in an attempt to express the effects of droplet size and flow rate with a single variable. The area flux can be defined based upon the SMD definition of (6) with the assumption that an individual spray droplet can be modeled as a sphere for the purposes of volume and surface area formulations.

$$A_{flux} = \frac{\dot{V}_{spray} * A_{spray}}{\dot{V}_{droplet}} = \frac{6\dot{V}_{spray}}{D_{32}} \tag{8}$$

The factor of six can be attributed to the formula for volume of a spherical droplet. Figure 22 illustrates the results of this parameterization.

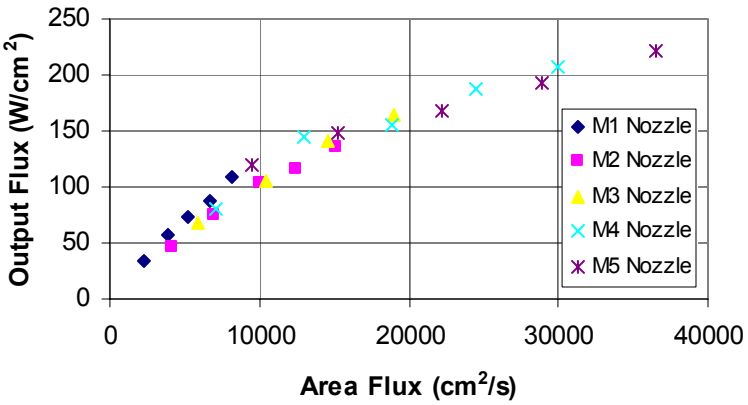

Figure 22. Heat Flux Dissipated versus Parameterized Variable Area Flux

The results indicate that A_{flux} is a suitable way of expressing the spray flow rate and droplet size in terms of a single variable. This variable provides some physical understanding of the rate at which the available heat transfer surface area is being replenished with cooling fluid. The largest value of flow rate and smallest droplet size within the range of data can be attributed to the M5 nozzle at 500 psi operational pressure. Earlier discussion has addressed the trend of increasing heat removal with increasing flow rates and decreasing droplet sizes. This is further emphasized with this parameterization.

The variable A_{flux} can be used to develop another parameter that can be used to gain a more physical understanding of the effectiveness of spray cooling as a heat transfer mechanism. By dividing the A_{flux} by the area of the heater element, the ratio A_{flux}/A_h is formed with dimensions of s^{-1} or the inverse of time. This time relative area ratio represents the surface area created by the individual droplets of the impinging spray relative to the surface area of the heater element. Table 5 summarizes these ratios for the experimental data.

SMD (micrometers)	Flow Rate (L/h)	A_{flux} (cm^2/s)	A_{flux}/A_h (s^{-1})
28.4	3.79	2221.24	280.56
22.6	5.34	3935.84	497.12
20.7	6.55	5272.95	666.00
18.7	7.58	6755.79	853.30
17.4	8.48	8121.65	1025.81
30.3	7.57	4164.47	526.00
25.8	10.71	6920.54	874.10
21.7	13.10	10059.91	1270.62
20.3	15.16	12446.63	1572.08
18.7	16.92	15081.11	1904.83
32.4	11.36	5841.56	737.82
25.5	16.05	10490.20	1324.97
22.4	19.68	14645.83	1849.85
19.9	22.76	19061.98	2407.64
35.5	15.14	7108.92	897.90
27.5	21.43	12984.85	1640.06
23.2	26.23	18845.55	2380.30
20.7	30.33	24420.29	3084.42
18.8	33.84	30001.77	3789.39
33.3	18.93	9472.97	1196.49
29.3	26.76	15223.55	1922.82
24.6	32.78	22210.03	2805.25
21.9	37.92	28858.45	3644.99
19.3	42.32	36546.63	4616.05

Table 5. Summary of Time Relative Area Ratios

These ratios show that the surface area created by the impinging spray droplets is on the order of up to several thousand times the heat transfer surface area attributed to the heater element. The inversely proportional relationship with time shown in the ratio is representative of the time necessary to achieve this increased surface area starting from the time the spray leaves the nozzle orifice. The large values of relative area ratios and the corresponding small times to achieve these elevated impinging spray surface areas further suggest the effectiveness of spray cooling as a means of heat flux removal.

E. COMPARISON WITH PREVIOUS WORKS

This study focused on spray cooling of a heated surface under steady state conditions using a series of commercially available full cone pressure nozzles capable of delivering flow rates from 3.79 L/h to 42.32 L/h and droplet sizes ranging from 17.4 μm to 35.5 μm. The maximum experimental heat flux dissipated was 221.2 W/cm^2. There

are very few works throughout the literature that paralleled the present work concerning the spray cooling of a heated surface in the nucleate boiling region of the boiling curve under steady state conditions.

The three experiments that are most comparable to the present work are those of Cryer (2003), Liu (2002) and Ortiz (1999). Cryer studied spray cooling of a heated surface in the nucleate boiling region under steady state conditions using full cone pressure nozzles that produced similar droplet sizes to the nozzles used in the present experiment (19 μm to 32 μm), but at significantly lower flow rates (2.05 L/h to 9.68 L/h). It is important to note that the parameters considered, spray droplet diameter and spray volumetric flow rate, were the same in both experiments. Although the trends represented in Cryer's data agree closely with the present data produced in the current experiment, the earlier experiment maximum extracted power density was 56.5 W/cm^2. This is approximately 25 percent of the maximum value obtained during this experiment. This large difference can be attributed to the significantly higher spray flow rates utilized during the present study as well as the reduced cross sectional area heater of the heater element that permitted a higher heat flux.

Liu (2002) also studied the parameters of volumetric flow rate (0.684 L/h to 22.86 L/h) and droplet size (12 μm to 198 μm), but focused on their effect on the critical heat flux (CHF). Unlike the pressure nozzles used in the present experiment, Liu utilized air assisted nozzles and developed the area flux correlation discussed in the previous chapter. The area flux was considered to be an effective in providing a physical sense of how well the heat transfer area is being replenished with cooling fluid and therefore providing a quantitative measure of the heat removal capacity of the system.

Gonzales (1999) conducted a thorough spray cooling experiment that studied the effects of surface roughness, degree of subcooling, impact angle, and flow rate on steady-state high heat fluxes. Full cone pressure nozzles producing flow rates ranging from 1.48 L/h to 2.91 l/h and droplet diameters between 85 μm and 100 μm were used for spray cooling resulting in steady state high heat fluxes in excess of 500 W/cm^2. The results indicated that the maximum achievable steady-state heat flux increased with mass flow rate and surface roughness, but decreased for an increase in impact angle and subcooling

degree. Although Gonzales did not study the effect of droplet size, the relationship between mass flow rate and heat flux found in the present study agreed with these previous results.

The majority of the works found in the literature focused on advanced nozzle technologies such as those which employ piezoelectric generators to break the water jet into a uniform droplet spray, ink-jet nozzle arrangements, and nozzles capable of sensing the highest temperature regions of a heat transfer surface and then targeting these particular hot spots as a result. Much attention was focused on a statistical analysis of the data that might ultimately provide a useful mathematical correlation that could accurately predict future spray cooling data. Many of these studies concentrated on determining the system CHF for the parameters under consideration. Operating in this region is advantageous as it provides a good indication of the maximum theoretical heat removal capacity of a system. It is considered dangerous due to the inherent instability associated with the large rise in temperature corresponding to a small increase in heat flux that takes place at the CHF. This experiment operated below the CHF to ensure the continuous and reliable operation of the experimental apparatus, but at a surface temperature significantly elevated to take maximum advantage of the two phase cooling in the nucleate boiling regime.

The results of the spray cooling experiments not explicitly discussed are summarized in Table 5 to include the parameters studied, nozzle and spray medium used, flow rates and droplet size, and maximum CHF value achieved.

Author	Nozzle Type	SMD	Flow Rate or Mass Flux	Parameters Studied	CHF (W/cm2)
Comini et al. [1979]	Full Cone	45-99 μm	N/A	SMD, T_e	220
Choi et al. [1987]	Piezo-electric	0.407-0.530 mm	01-0.16 g/s cn	SMD, V_{drop} Mass Flux	350
Pais et al. [1992]	Air Assisted	7.2-28.4 μm	1.4-5.1L/h	SMD, Flow Rate Surface Rougness T_{sub}	650
Bonacina et al. [1979]	Air Assisted	300-500 μm	N/A	$V_{drop,}$ SMD	220
Halvorson et a [1994]	17-22 guage needle	2.3-3.8 mm	0.07 L/h	SMD, T_{sub} V_{drop}	170
Mudawar et al. [1996]	Full Cone	N/A	0.23 L/h	Nozzle-Surface Distance, T_{sub}	100
Webb et al. [1992]	Full Cone Air Assisted	32-56 μm	0.03-6.1 kg/m^2	SMD, V_{drop} Mass Flux	150
Toda [1971]	Air Assisted	88-146 μm	2.92 L/h	SMD, V_{drop} T_{sub}	600
Xia [2002]	Piezo-electric	100-300 μm	N/A	V_{drop}	924
Marcos et al. [2002]	Full Cone Air Assisted	N/A	0.17-0.50 L/h	$T_{sub,}$ Flow Rate	400

Table 6. Previous Spray Cooling Studies

Table 5 shows that the majority of the previous spray cooling experiments in the literature also used distilled water as the cooling fluid and many performed testing over a range of droplet diameters that can be considered comparable to the present work. None of these works however, include the large range of flow rates studied in this experiment. Although heat flux, not the CHF, was studied in the present work it can be seen that the maximum heat flux achieved (221 W/cm^2) exceeds the CHF values achieved in several of the earlier studies. The largest CHF values of 650 W/cm^2 and 924 W/cm^2 attributed to Pais et al. and Xia, respectively were achieved using air assisted and piezo-electric

nozzles. These types of spray nozzles are capable of higher heat flux removal than full cone pressure nozzles due to their ability to produce a refined and precisely controlled spray.

F. PREDICTIVE CORRELATION OF RAW DATA

The experimental data was compared to a predictive correlation for the critical heat flux developed by Estes (1995). Estes conducted spray cooling experiments with water FC-72, and FC-87 with spray nozzles that produced full cone pressure sprays similar to the spray patterns produced in the current experiment. Estes' work differed from the present study with regard to the relatively large SMD values used-110-225 micrometers, and the proximity to which he operated near the critical heat flux. Based on the CHF experimental data, Estes developed a correlation with respect to the local volumetric flux and the SMD:

$$q'' = (\rho_g h_{fg} Q'') * 2.3 \left(\frac{\rho_f}{\rho_g} \right)^{0.3} \left(\frac{\rho_f Q''^2 d_{32}}{\sigma} \right)^{-0.35} * \left(1 + 0.019 \frac{\rho_f c_{p,f} \Delta T_{sub}}{\rho_g h_{fg}} \right) \quad (9)$$

Figure 22 illustrates the results of applying Estes' CHF correlation to the data from the present study.

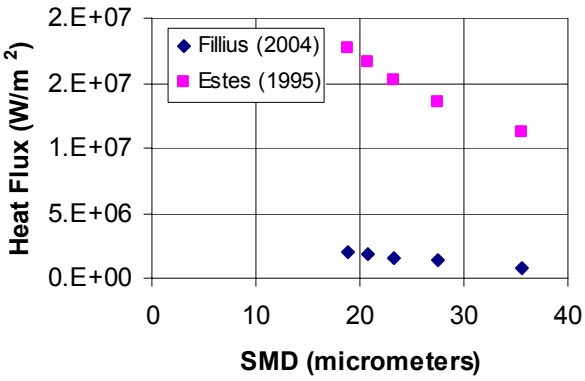

Figure 23. Comparison of M4 Nozzle Data with Estes Correlation

Figure 23 clearly illustrates the incompatibility between the correlation and the present study. The large discrepancy can likely be attributed to the large variation

between the droplet diameters used in the two experiments. It is important to note that Estes concentrated particularly on operating at the CHF, while the present experiment operated farther below this value in an effort to produce good spray conditions while ensuring system integrity.

In an effort to formulate a mathematical correlation that would accurately predict heat flux dissipation rates for water spray cooling, the two independent parameters of volumetric flow rate and droplet diameter studied during this experiment were addressed separately. First the data used to develop the constant flow rate/SMD relationships illustrated in Figures 17 and 20 respectively, was manipulated such that the ratios of the SMD's in the constant flow case and ratios of the flow rates in the constant SMD case were formed and then plotted against the corresponding heat flux ratios. These relationships are shown in Figure 23 and 24.

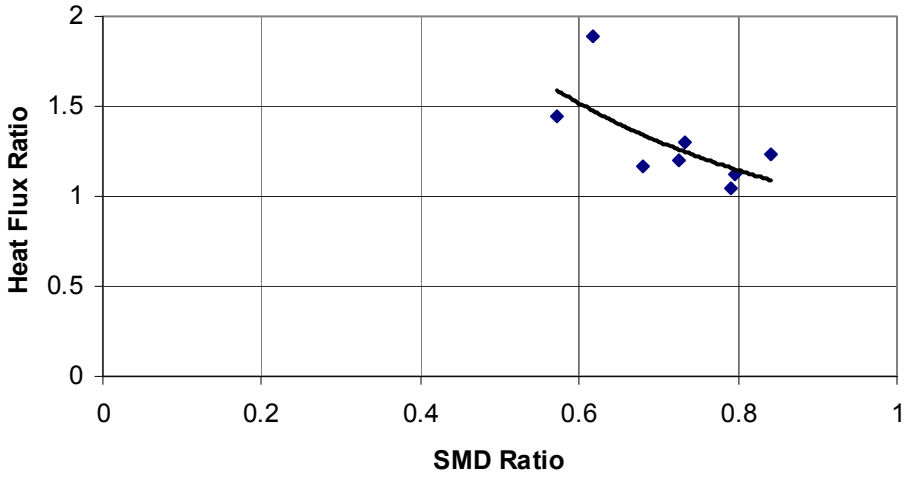

Figure 24. Heat Flux/SMD Predictive Correlation (constant flow rate)

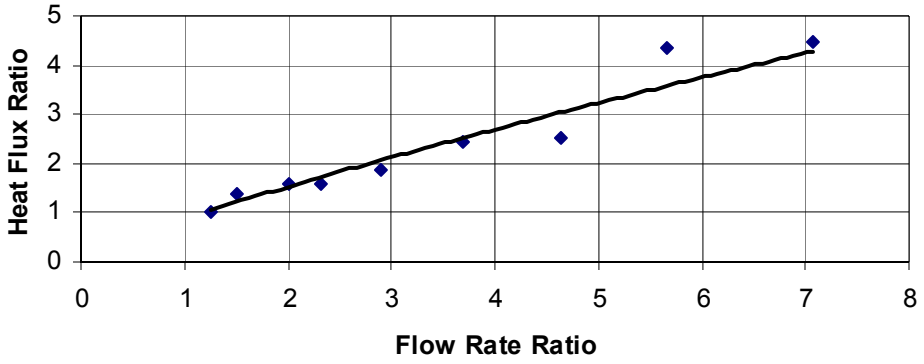

Figure 25. Heat Flux/Flow Rate Predictive Correlation (constant SMD)

The results of this analysis provide two separate expressions for the purpose of formulating a predictive correlation. The first predicts heat flux in terms of the droplet size for constant flow conditions:

$$q_{ratio}^{"} = 0.9206 d_{32_{ratio}}^{-0.9773} \tag{10}$$

The second expression correlates heat flux for constant droplet diameter cases with respect to flow rate:

$$q_{ratio}^{"} = 0.8675 \dot{V}_{ratio}^{0.817} \tag{11}$$

The specific data used in formulating these ratios is shown In Tables 6 and 7.

Pressure (psi)	Flow Rate (L/h)	SMD micrometers	Output Flux (W/cm2)	Flow Ratio	Flux Ratio
M1/400	7.58	18.7	87.117	2.23	1.55
M2/500	16.921	18.7	135.321	2.00	1.53
M4/500	33.842	18.8	207.469	4.46	2.38
M2/300	13.098	21.7	103.603	2.90	1.86
M5/400	37.92	21.9	192.322		
M1/200	5.337	22.6	57.675	3.69	2.45
M3/300	19.684	22.4	141.272		
M3/200	16.05	25.5	104.532	1.50	1.38
M2/200	10.713	25.8	75.519		
M4/400	30.33	20.7	186.702	2.00	1.60
M2/400	15.16	20.3	116.738	2.31	1.58
M1/300	6.549	20.7	73.843	4.63	2.53
M5/200	26.763	29.3	148.126	7.07	4.46
M1/100	3.785	28.4	33.183	5.66	4.35
M4/200	21.425	27.5	144.499	1.25	1.03

Table 7. Flow and Flux Ratio Data for Constant SMD Cases

Pressure (psi)	Flow Rate (L/h)	SMD micrometers	Output Flux (W/cm^2)	SMD Ratio	Flux Ratio
M1/400	7.58	18.7	87.117	0.62	1.00
M2/100	7.57	30.3	46.002		
M4/300	26.233	23.2	154.601		
M5/200	26.763	29.3	148.126	0.79	0.98
M2/200	10.713	25.8	75.519	0.80	0.94
M3/100	11.356	32.4	67.301		
M2/500	16.921	18.7	135.321	0.73	1.05
M3/200	16.05	25.5	104.532		
M4/100	15.14	35.5	80.794	0.84	1.00
M3/165	15.15	29.9	100.0386329	0.68	1.00
M2/400	15.16	20.3	116.738	0.57	1.00
M3/400	22.76	19.9	165.092	0.73	1.00
M4/210	22.75	27.4	138.1544987		

Table 8. SMD and Flux Ratio Data for Constant Flow Cases

Equations (10) and (11) represent two separate correlations for the heat flux ratio: one in terms of flow rate for a constant SMD, and the other in terms of SMD for a constant flow rate. In an effort to obtain a single formula for heat flux in terms of both parameters to serve as a suitable correlation for the data, the following expression was assumed for the correlation based on the results of (10) and (11):

$$q'' = C\dot{V}^{m} D_{32}{}^{n} \tag{12}$$

where C is a constant to be determined, m=0.7299 and n=-0.8044. The values for m and n were obtained through the use of curve fitting software. The software was used to drive the coefficients of the power expressions of (10) and (11) toward unity to provide a sound physical basis for the predictive correlation in (12). Coefficients m and n are the results of fitting the ratio data used in formulating (10) and (11) to expressions with unity as the leading coefficient. Experimental values of the heat flux were plotted against the product of V^m and $D_{32}{}^n$ for the experimental values of flow rate and droplet size. A linear fit was applied to the data and the slope predicted by this linear fit was taken to be the value of the constant C. Figure 25 illustrates the results of the linear fit.

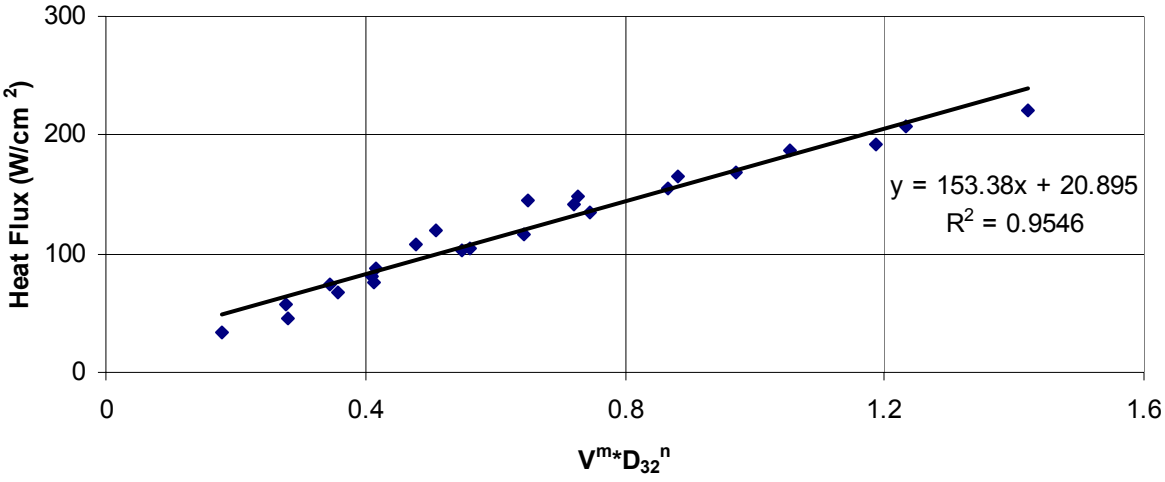

Figure 26. Linear Fit for Correlation Data

The correlation predicted in (12) was then applied to the experimental data to measure its effectiveness in predicting heat flux due to spray cooling. Figure 26 shows the comparison between the experimental and correlated heat flux values for the M5 nozzle. The correlation predicts the heat flux within an average of 18.5% of the experimental value.

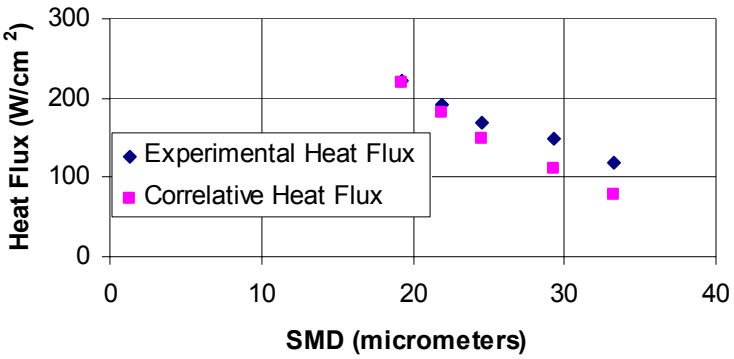

Figure 27. Comparison Between Experimental and Correlative Heat Flux-M5 Nozzle

G. MODIFIED PREDICTIVE CORRELATION

Comini et al. (1979) analyzed the heat transfer mechanisms associated with spray cooling and developed a mathematical model based on the assumption of dropwise evaporation from the heater surface. The heat transfer rate through an individual spray droplet from the heat transfer surface is expressed while taking into account the contribution due to sensible heat during the process:

$$q''_d = \left[\frac{\rho_l \bullet \dot{V}_{spray}}{A_{heater}}\right]\left[h_{fg} + b_1 c_{pl}\left(T_h - T_l\right)\right] \tag{14}$$

Comini et al. (1979) also developed a dimensionless parameter termed the wetted fraction or the fraction of heat transfer area covered by droplets. This parameter was applied to the present data by forming the ratio of experimental heat flux to the heat flux dissipated in (13). This ratio can be thought of as the percentage of the heat transfer area covered by spray cooling droplets and for the case of b_1 equal to one in (13), experimental values of the wetted fraction ranged from 5-10 percent.

As spray droplets impinge upon and then form a thin liquid film on a heater surface through which heat transfer occurs, inertial forces and surface tension play a vital

role in the behavior of that heat transfer process. The Weber number is a dimensionless parameter forming a ratio of the inertial to surface tension forces.

$$We = \frac{\rho(\dot{V}_{spray} / A_h) D_{32}}{\sigma} \tag{15}$$

The wetted fraction number was plotted against Weber number for the experimental data, but M1 nozzle data was disregarded in this case because of its error margins. The reason for considering the data produced during runs with this particular nozzle as outlying data can be attributed to the difficulty of maintaining the desired pressure set point during these relatively low spray flow rates. The relationship between wetted fraction and wetted fraction is shown in Figure 28.

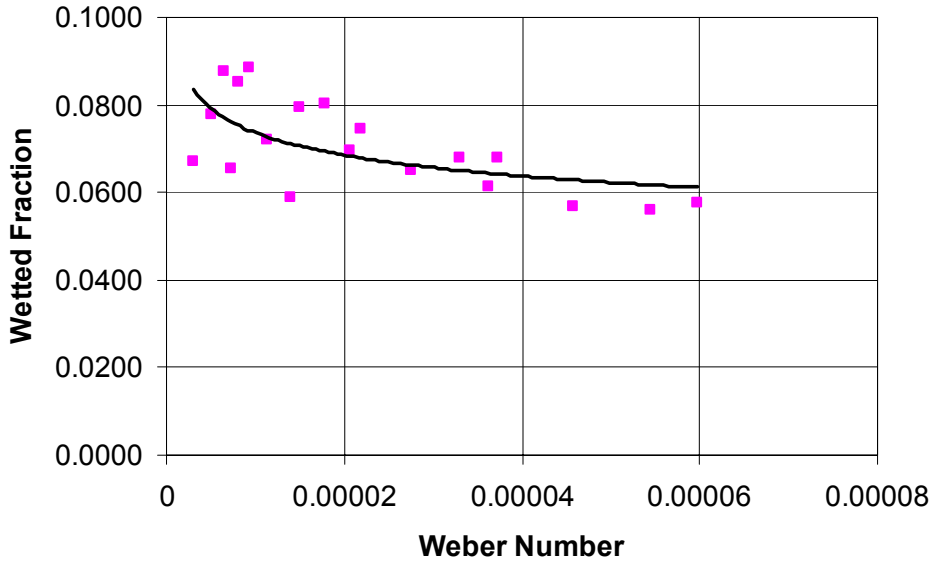

Figure 28. Relationship Between Wetted Fraction and Weber Number

A least squares analysis was applied to the data and a correlation between the two parameters was developed.

$$\varepsilon = 0.0222 We^{-0.1041} \tag{16}$$

The correlation developed in (13) compares with the experimental data within an average of 9.54%.

THIS PAGE INTENTIONALLY LEFT BLANK

V. CONCLUSIONS

An experimental study has been performed to determine how the parameters of volumetric flow rate and droplet size affect the heat dissipation for spray cooling in the nucleate boiling regime under steady-state conditions. Spray nozzles were used for water flow rates in the range of 3.79 to 42.32 L/h with droplet sizes from 17.4 to 35.5 micrometers. A maximum value of 221.2 W/cm^2 was achieved for steady-state heat flux.

The results of the experiment indicate that heat flux is dependent upon both the volumetric flow rate and droplet size of a cooling spray. The data shows that heat flux increases with increasing flow rate and decreases with increasing values of the spray diameter. These trends are consistent with previous work and were emphasized by studying each parameter independently. A correlation for the present data was developed to predict the experimental heat flux as a function of flow rate and droplet diameter. This correlation compared with the experimental values within an average of 18 percent. A modified correlation between the dimensionless Weber number and wetted fraction was developed that compared with the experimental data within 9 percent.

Recommendations for future work to expand upon the present study include the investigation of spray cooling utilizing advanced nozzle technology such as piezo-electric excitation or ink-jet nozzle arrangements. Experimentation involving the study of the effects of subcooling, reduced gravity, and higher heat transfer surface temperatures would provide a more robust understanding of spray cooling effectiveness. More work is necessary to develop mathematical spray cooling correlations that can accurately predict heat flux dissipation for a wide range of parameters, ultimately reducing the need for further testing and experimentation.

THIS PAGE INTENTIONALLY LEFT BLANK

APPENDIX A. EQUIPMENT AND MATERIAL SPECIFICATIONS

A. VARIABLE VOLTAGE TRANSFORMER

Manufacturer: Staco

Model: 5021 CT, closed case

Input Voltage: 200 Volts/60 Hz AC

Output Voltage: 0-237 Volts (peak-to-peak)

Maximum Current: 28 Amps

B. THERMAL EPOXY FILLING THERMOCOUPLE HOLES

Manufacturer: Omega

Model: OB-200 Epoxy Adhesive

Thermal Conductivity: 1.26 W/m-K

Tensile Shear Strength: 190 kg/cm^2, at 24 C, 148 kg/ cm^2 at 149 C

Coefficient of Thermal Expansion: $38*10^{-6}$ in/in/C

Maximum Continuous Temperature: 260 C

C. CARTRIDGE HEATERS

Manufacturer: Watlow

Model: J3A79-L12

Length: 3 in., Diameter: 0.496+/-0.005 in.

Capacity: 1000 W nominal power at 120 Volts

Resistance: 14 Ohms, nominal

D. THERMOCOUPLES

Manufacturer: Omega

Model: Type E, 5SRTC-KK-E-30-36

Bead Diameter: 0.010 in.

E. PRESSURE GAGE

Manufacturer: Omega

Model: DPG500-1K-D2

Range: 0-1000 psi

Output: Digital Display, 0-5 VDC analog output to data acquisition unit

Calibration: 0.25% FS (+/-2.5 psi)

F. NOZZLES

Manufacturer: Hago Precision Nozzles

Models: M1, M2, M3, M4, M5

Flow Characteristics: Sauter mean diameters and volumetric flow rates for range of experimental operational pressures displayed in Tables 3 and 4, respectively.

G. THERMAL COMPOUND IN CARTRIDGE HEATER AIR GAPS

Manufacturer: J. B. Weld Company

Model: 8265-S

Maximum Operating Temperature: 315 C

Tensile Strength: 3960 psi

APPENDIX B. FLUID AND HEATER ELEMENT PROPERTIES

Properties of Pure Copper

k = 401 W/m-K

Properties of Distilled Water at 28 C

ρ_l = 1000 kg/m^3

ρ_v = 598 kg/m^3

h_{fg} = 2256 kJ/kg

σ = 0.0712 N/m

c_{pl} = 4.218 kJ/kg-K

THIS PAGE INTENTIONALLY LEFT BLANK

APPENDIX C. TABULATED EXPERIMENTAL DATA

Nozzle Type	Pressure (psi)	Flow Rate (L/h)	SMD (micrometers)	Heat Dissipated (W/cm^2)
M1	100	3.785	28.4	33.183
M1	200	5.337	22.6	57.675
M1	300	6.549	20.7	73.843
M1	400	7.58	18.7	87.117
M1	500	8.479	17.4	108.428
M2	100	7.571	30.3	46.002
M2	200	10.713	25.8	75.519
M2	300	13.098	21.7	103.603
M2	400	15.16	20.3	116.738
M2	500	16.921	18.7	135.321
M3	100	11.356	32.4	67.301
M3	200	16.05	25.5	104.532
M3	300	19.684	22.4	141.272
M3	400	22.76	19.9	165.092
M4	100	15.142	35.5	80.794
M4	200	21.425	27.5	144.499
M4	300	26.233	23.2	154.601
M4	400	30.33	20.7	186.702
M4	500	33.842	18.8	207.469
M5	100	18.927	33.3	119.275
M5	200	26.763	29.3	148.126
M5	300	32.782	24.6	168.18
M5	400	37.92	21.9	192.322
M5	500	42.321	19.3	221.196

Table 9. Summary of Experimental Data

THIS PAGE INTENTIONALLY LEFT BLANK

APPENDIX D. SAMPLE CALCULATIONS

A. SURFACE HEAT FLUX CALCULATION FOR M5 AT 500 PSI

The surface heat flux was calculated by applying Fourier's Law for Heat Conduction along the axial direction of the reduced area section of the heater element. T_1, T_2, T_3 are the temperatures sensed by thermocouples placed at the uppermost axial position spaced at 120 degree circumferential locations on the heater element. T_7, T_8, T_9 are the temperatures sensed by thermocouples at the lowermost axial position from the heater element surface at spaced circumferntially at the same interval as the three uppermost temperatures. dx is the separation between these two axial thermocouple placements, and k is the thermal conductivity of pure copper given as 4.01 W/cm-K.

$$q'' = k\frac{dT}{dx}$$

$$dT = \left[\frac{T_7 + T_8 + T_9}{3}\right] - \left[\frac{T_1 + T_2 + T_3}{3}\right]$$

$$dT = \left[\frac{200.22 + 203.02 + 200.73}{3}\right] - \left[\frac{165.49 + 166.15 + 167.25}{3}\right] = 35.03K$$

$$q'' = 4.01W/cm^2\left(\frac{35.03K}{0.635cm}\right)$$

$$q'' = 221.20W/cm^2$$

THIS PAGE INTENTIONALLY LEFT BLANK

APPENDIX E. THERMOCOUPLE CHANNEL ASSIGNMENTS

Channel 0: Distilled Water Temperature Prior to Entering Nozzle
Channel 1: Heater Element Uppermost Axial Location at 0 degrees
Channel 2: Heater Element Uppermost Axial Location at 120 degrees
Channel 3: Heater Element Uppermost Axial Location at 240 degrees

Channel 4: Heater Element Central Axial Location at 0 degrees
Channel 5: Heater Element Central Axial Location at 120 degrees
Channel 6: Heater Element Central Axial Location at 240 degrees

Channel 7: Heater Element Lowermost Axial Location at 0 degrees
Channel 8: Heater Element Lowermost Axial Location at 120 degrees
Channel 9: Heater Element Lowermost Axial Location at 240 degrees

All axial locations referenced to surface of heater element.

THIS PAGE INTENTIONALLY LEFT BLANK

LIST OF REFERENCES

A. Marcos, L.C. Chow, J.H. Du, S. Lei, D.P. Rini, and J.L. Lindauer, Spray Cooling at Low System Pressures, *18th IEEE SRMI-THERM Symposium*, pp. 169-175, 2002.

B.W. Webb, M. Queiroz, K.N. Oliphant, and M.P. Bonin, Onset of Dry-Wall Heat Transfer in Low Mass Flux Spray Cooilng, *Journal of Experimental Heat Transfer*, vol. 5, pp. 33-50, 1992.

C. Xia, Spray/Jet Cooling for High Heat Flux to 1 kW/cm2, 18th IEEE SEMI-THERM Symposium, pp. 159-163, 2002.

F. P. Incropera, D. P. De Witt, Fundamentals of Heat and Mass Transfer, Third Edition, 1990.

G. Comini, S. D. Giudice, Dropwise Evaporation, *Journal of Heat Transfer*, vol. 101, pp. 441-446, 1979.

J. D. Bernardin, C. J. Stebbins, I. Mudwar, Effects of Surface Roughness on Water Droplet Impact History and Heat Transfer Regimes, *International Journal Heat Mass Transfer*, vol. 40, no. 1, pp. 73-88, 1997.

J. Schmidt, H. Boye, Influence of Velocity and Size of the Droplets on the Heat Transfer in Spray Cooling, *Chemical Engineering Technology*, vol. 24, pp. 255-260, 2001.

K. A. Estes, I. Mudawar, Correlation of Sauter Mead Diameter and Critical Heat Flux for Spray Cooling of Small Surfaces, *International Journal Heat Mass Transfer*, vol. 38, no. 16, pp. 2985-2996, 1995.

K. J. Choi, S. C. Yao, Mechanisms of Film Boiling Heat Transfer of Normally Impacting Spray, *International Journal Heat Mass Transfer*, vol. 30, no. 2, 1987.

L. Gonzales and J.I. Gonzales, Experiments on Steady-State High Heat Fluxes Using Spray Cooling, *Experimental Heat Transfer*, vol. 12, pp. 215-233, 1999.

M. A. Cryer, An Experimental Study of High Heat Flux Removal Using Micro-Droplet Spray Cooling, Master's Thesis, Naval Postgraduate School, Monterey, California, 2003.

M.G. Cooper, J. P. Lloyd, Transient Local Heat Flux in Nucleate Boiling, *International Heat Transfer Conference*, vol. 3, pp. 193-203, 1966.

M. R. Pais, E. T. Mahefkey, and L.C. Chow, Surface Roughness and Its Effects on the Heat Transfer Mechanisms in Spray Cooling, *Journal of Heat Transfer*, vol. 114, pp. 211-219, 1992.

M. S. Sehmbey, L.C. Chow, M. R. Pais, T. Mahefkey, High Heat Flux Spray Cooling: A Review, *Heat Transfer in High Heat Flux Systems ASME 1994*, vol. 301, 1994.

M. S. Sehmbey, L.C. Chow, M. R. Pais, T. Mahefkey, High Heat Flux Spray Cooling of Electronics, *American Institute of Physics Conference 950110*, pp. 903-909, 1995.

P.J. Halvorson, R. J. Carson, S. M. Jeter, and S. I. Abdel-Khalik, Critical Heat Flux Limits for a Heated Surface Impacted by a Stream of Liquid Droplets, *Journal of Heat Transfer*, vol. 116, pp. 675-685, 1994.

R. E. Gaugler, An Experimental Study of Spray Cooling of High Temperature Surfaces, Ph. D Thesis, Carnegie Institute of Technology, Pittsburg, 1966.

R. Mesler, Surface Roughness and Its Effects on the Heat Transfer Mechanism of Spray Cooling, *Journal of Heat Transfer*, vol. 115, pp. 1083-1085, 1993.

S. Toda, A Study of Mist Cooling (1st Report: Investigation of Mist Cooling), *Heat Transfer-Japan*, vol. 1, pp. 39-50, 1971.

W. M. Rosenhow, A Method of Correlating Heat Transfer Data for Surface Boiling Liquids, *Trans. ASME*, vol. 74, 1985.

Z. Liu, Experimental Study of the Boiling Critical Heat Flux of Mist Cooling, *Experimental Heat Transfer*, vol. 15, pp. 229-243, 2002.

THIS PAGE INTENTIONALLY LEFT BLANK

INITIAL DISTRIBUTION LIST

1. Defense Technical Information Center
   Ft. Belvoir, Virginia

2. Dudley Knox Library
   Naval Postgraduate School
   Monterey, California

3. Ashok Gopinath
   Naval Postgraduate School
   Monterey, California

4. James Fillius
   Naval Postgraduate School
   Monterey, California

5. Anthony Healey
   Naval Postgraduate School
   Monterey, California